ASSEMBLY OF INTERFERENCE FITS

BY IMPACT AND CONSTANT FORCE METHODS

by

CRAIG C. SELVAGE

S.B., Massachusetts Institute of Technology
(1978)

SUBMITTED IN PARTIAL FULFILLMENT
OF THE REQUIREMENTS FOR THE
DEGREE OF

MASTER OF SCIENCE

AT THE

MASSACHUSETTS INSTITUTE OF TECHNOLOGY

JUNE, 1979

Signature of Author . . . . . .
Department of Mechanical Engineering, May 11, 1979

Approved by . . . . . .
Technical Supervisor, CSDL

Certified by . . . . . .
Thesis Supervisor

Accepted by . . . . . .
Chairman, Department Committee on Graduate Students

ASSEMBLY OF INTERFERENCE FITS BY IMPACT AND CONSTANT FORCE METHODS

by

CRAIG C. SELVAGE

Submitted to the Department of Mechanical Engineering

on May 11, 1979 in partial fulfillment of the requirements

for the degree of Master of Science

ABSTRACT

This thesis investigates the assembly of interference fits by the two basic methods. The parts may be pressed together quasi-statically, under a constant load, or be driven into place with a series of impacts.

When the parts are pressed together, the important consideration is the static insertion force. Handbook formulas give an approximate value for the insertion force because the coefficient of friction is not known with certainty, and the assumed constant contact pressure is altered by the axial force through the Poisson effect.

This thesis accounts for the Poisson effect, and shows that it becomes an important consideration when the product of Poisson's ratio, coefficient of friction, and the contact length to interference diameter ratio exceeds 0.1.

The residual axial stresses resulting from assembly forces are analyzed in detail, and the minimum energy which must be supplied to begin insertion is calculated.

An approximate energy analysis of the insertion of an interference fit by an impact load is presented. This analysis takes into account the presence of an axial preload force which might be applied as the impact takes place. Two experiments show a good correlation between the theory and data for impact by hammer blows.

Thesis Supervisor: Dr. Daniel E. Whitney, Lecturer,
Department of Mechanical Engineering

ACKNOWLEDGMENTS

This thesis was prepared at the Charles Stark Draper Laboritory, Inc., with funding provided by the National Science Foundation grant number APR74 - 18173 A03.

I thank my thesis supervisor, Dr. Daniel E. Whitney for the advice, help, and discussions he contributed, and Valerie Naves for her help in typing this document.

TABLE OF CONTENTS

LIST OF FIGURES

LIST OF TABLES

1.0 INTRODUCTION

The analysis presented in this thesis was developed in support of research on industrial assembly[1]. Of fundamental importance is the study of parts mating science. The basic purpose of parts mating science is to understand the phenomena which occur as parts are assembled or mated. This requires the construction of mathematical models which describe the geometric and force relationships as the parts are assembled.

An analysis of the insertion of a round peg into a hole with a relative clearance has yielded theories which describe the conditions under which jamming or wedging can be avoided during the assembly process. Guided by this analysis, a device called a Remote Center Compliance has been developed which allows rapid and jam-free insertion of close clearance parts having chamfers[2].

This thesis investigates the assembly of parts having a negative clearance, called interference, press, or force fits. This type of fit is commonly used for assembling bearings, attaching gears or sprockets to shafts, inserting dowel pins into holes, and holding bushings into housings. Often they are used in place of splines, keyways, and fasteners, permitting a simpler, less costly design, with improved stress distribution.

There are two general methods of interference fit assembly. The parts may be pressed together quasi-statically, under constant force, or driven into position using a series of impacts. Unfortunately, from the assembly point of view, the force required to press together an interference fit ranges from several to many thousands of pounds. An assembly machine or robot may not have sufficient load capacity to perform the insertion by directly pressing the parts together. Thus, assembly by impact (such as with a pneumatic hammer) promises to be an attractive alternative.

This research provides a method for calculating the insertion force associated with a particular interference fit, and presents an approximate analysis for predicting the insertion distance provided by a given hammer blow. Useful for the design of interference fits are equations for withdrawal, or holding force, which

in general, differs from the insertion force. The analysis of assembly by impact may also be used to determine the impact absorbing capability of an interference fit subjected to service loads which are impulsive in nature.

2.0 INSERTION AND WITHDRAWAL FORCES

An interference fit is obtained by forcing a shaft into a hole with a slightly smaller diameter. To accommodate this interference, the shaft must contract radially, and the hole expand, producing a radial contact stress at the interface. This radial stress is referred to in the literature as an "interference pressure", and this term is used here. In general, the interference pressure varies along the length of contact, and changes in response to the external loading of the assembled interference fit.

The force necessary to produce relative sliding between the parts (insertion or withdrawal force), is the product of the coefficient of friction and the surface integral of the contact pressure.

The most simple case to consider is that of two interfering concentric cylinders of equal length, where the inner cylinder is fully enclosed by the outer. In the absence of axial stresses, each cylinder is in a state of plane stress, and the interference pressure is constant along the length of contact. The application of an axial insertion force, however, will produce a variation in the interference pressure due to the Poisson effect of axial stresses.

The traditional treatments of interference fits found in texts and handbooks[3-7] always assume a constant interference pressure (equal length fully engaged cylinders), and neglect the Poisson effect of axial stresses. Thus, these equations only approximate the case of a hub fit on a long shaft, or a partially inserted shaft, where the interference pressure forms a concentration at the edges of contact. In these cases where edge discontinuities exist, there are no exact analytic solutions, so finite element methods[8-11] are used when the interference pressure distribution must be known with accuracy. The handbook equations are usually of practical value, however, because the uncertainty due to the coefficient of friction is likely to be larger than the error resulting from the constant pressure assumption.

First, the equations for the constant pressure approximation are given. Then, the Poisson effect of axial stress will be accounted for, and finally the effect of pressure concentrations will be examined.

2.1 Approximate Equations

Given two fully engaged cylinders with a constant radial interference of δ, the outer cylinder (designated by o) must increase its inner radius by δ_o, and the inner cylinder (designated by i) must decrease its outer radius by δ_i. Tangential strain at a radius r is given by:

$$\varepsilon_t = \frac{\text{change in circumference}}{\text{original circumference}} = \frac{2\pi(r + \Delta r) - 2\pi r}{2\pi r} = \frac{\Delta r}{r} \tag{2.1}$$

Thus, assuming elastic materials,

$$\delta_o = b\varepsilon_{to} = \frac{b}{E_o}(\sigma_{to} + \nu_o p) \tag{2.2}$$

$$\delta_i = -b\varepsilon_{ti} = \frac{-b}{E_i}(\sigma_{ti} + \nu_i p) \tag{2.3}$$

where b = radius to interference

p = radial interference pressure

σ_t, ε_t = tangential stress and strain

E = Young's modulus

ν = Poisson's ratio

The Lamé stress equations[12] give the following expressions for tangential stress at the interference radius b:

$$\sigma_{to} = \left(\frac{c^2 + b^2}{c^2 - b^2}\right) p \tag{2.4}$$

$$\sigma_{ti} = -\left(\frac{b^2 + a^2}{b^2 - a^2}\right) p \tag{2.5}$$

where a = inner radius of inner cylinder

c = outer radius of outer cylinder

Substituting these into Eqs. (2.2) and (2.3), and utilizing the constraint $\delta = \delta_i + \delta_o$,

$$\delta = \frac{bp}{E_o}\left(\frac{c^2 + b^2}{c^2 - b^2} + \nu_o\right) + \frac{bp}{E_i}\left(\frac{b^2 + a^2}{b^2 - a^2} - \nu_i\right) \tag{2.6}$$

Solving for the interference pressure,

$$p = 1/2\ (\frac{\delta}{b})E_e \tag{2.7}$$

where

$$E_e = \frac{2}{\frac{1}{E_o}\left(\frac{c^2 + b^2}{c^2 - b^2} + \nu_o\right) + \frac{1}{E_i}\left(\frac{b^2 + a^2}{b^2 - a^2} - \nu_i\right)} \tag{2.8}$$

If the cylinders have the same material properties, E and ν,

$$E_e = \frac{E}{\left(\frac{b^2}{b^2 - a^2}\right) + \left(\frac{b^2}{c^2 - b^2}\right)}\ . \tag{2.9}$$

In addition, if a = o (solid shaft),

$$E_e = (1 - \frac{b^2}{c^2})E \tag{2.10}$$

By assuming the interference pressure remains constant in the presence of axial stresses, the insertion/withdrawal force, F, equals the product of interference pressure, contact area, and coefficient of friction.

$$F = p(2\pi bL)\mu \tag{2.11}$$

where L = length of contact

μ = coefficient of friction

Using Eq. (2.7) for the interference pressure,

$$F = \mu L(\pi \delta E_e) \tag{2.12}$$

If the interference, δ, is sufficiently large, the material will yield or fracture. For a ductile material, yield will occur when the maximum shear stress approaches one-half the tensile yield strength, σ_y, of the material. The maximum shear stress occurs at the inner surface of the outer cylinder and is given by:

$$\tau_{max} = \frac{p + \sigma_{to}}{2} \tag{2.13}$$

Using Eq. (2.4),

$$\tau_{max} = \frac{p}{1 - \frac{b^2}{c^2}} \tag{2.14}$$

For a solid shaft inside a collar of identical material and any outer diameter, the maximum allowable interference ratio is found from Eqs. (2.7, 2.10, and 2.14).

$$\frac{\delta_{max}}{b} = \frac{\sigma_y}{E} \tag{2.15}$$

For plain carbon steel, with a yield strength of 52,000 psi, the maximum interference ratio is 0.0017.

2.2 Poisson Effect of Axial Stresses

The following analysis takes axial stress into account and thereby considers the effect of axial loads on the interference pressure. Once again, equal length fully engaged cylinders are considered. The axial stress in each cylinder is assumed constant on any plane cross section, a function of axial direction only.

Four possible loading conditions may be examined, as shown in Figure 2.1. The derivations for the first two cases (insertion force) are presented here. The equations for withdrawal force are found by changing the appropriate algebraic signs.

CASE #1

The forces acting on a section of the inner cylinder are shown in Figure 2.2 where σ is positive for compressive axial stress. Equilibrium of forces requires that:

$$p(z) = \frac{b^2 - a^2}{2b\mu} \frac{d\sigma_i(z)}{dz} \tag{2.16}$$

If a section through both cylinders is taken, Figure 2.3, equilibrium, implies

$$\sigma_o(z) = \frac{A_i}{A_o} (\sigma_i(L) - \sigma_i(z)) \tag{2.17}$$

where A_i, A_o = cross-sectional areas.

The insertion force is given by $A_i\sigma_i(L)$. With the inclusion of the axial stresses, Eq. (2.6) becomes:

$$\delta = \frac{bp(z)}{E_o} \left(\frac{c^2 + b^2}{c^2 - b^2} + \nu_o \right) + \frac{bp(z)}{E_i} \left(\frac{b^2 + a^2}{b^2 - a^2} - \nu_i \right) + \frac{b\nu_o}{E_o} \sigma_o(z) - \frac{b\nu_i}{E_i} \sigma_o(z) \tag{2.18}$$

Substituting Eqs. (2.8, 2.16, and 2.17) into Eq. (2.18), the following differential equation for $\sigma_i(z)$ is obtained:

$$\left(\frac{b^2 - a^2}{\mu b E_e} \right) \frac{d\sigma_i(z)}{dz} - \left(\frac{\nu_i}{E_i} + \frac{\nu_o A_i}{E_o A_o} \right) \sigma_i(z) + \left(\frac{\nu_o A_i}{E_o A_o} \sigma_i(L) - \frac{\delta}{b} \right) = 0 \tag{2.19}$$

INSERTION FORCES

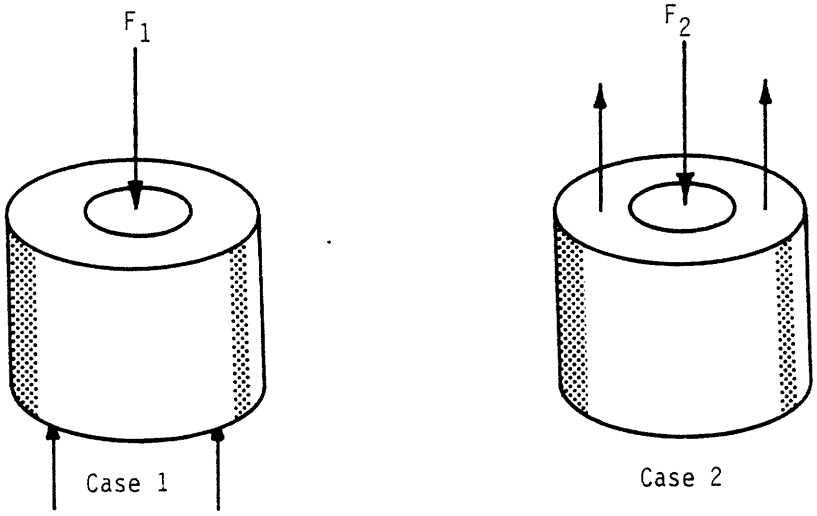

WITHDRAWAL FORCES

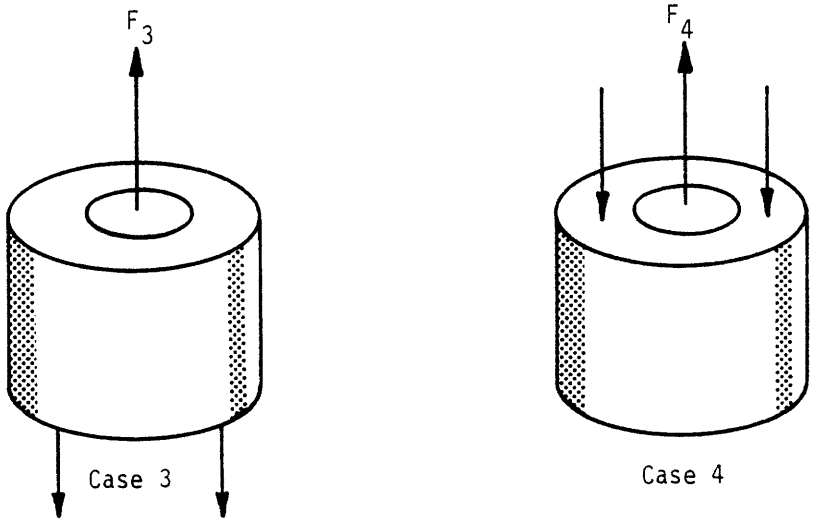

Figure 2.1

Possible axial loads

Figure 2.2

Forces acting on a thin section of inner cylinder.

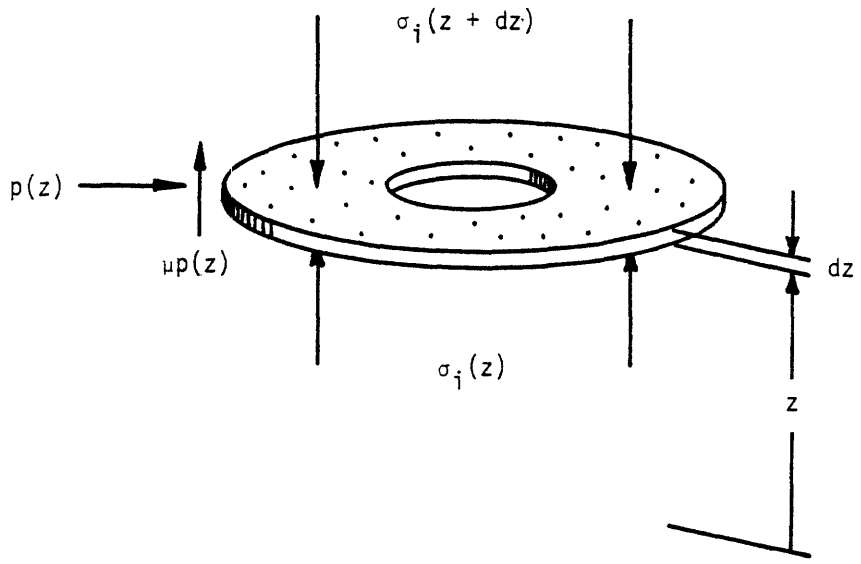

Figure 2.3

Forces acting on inner and outer cylinders.

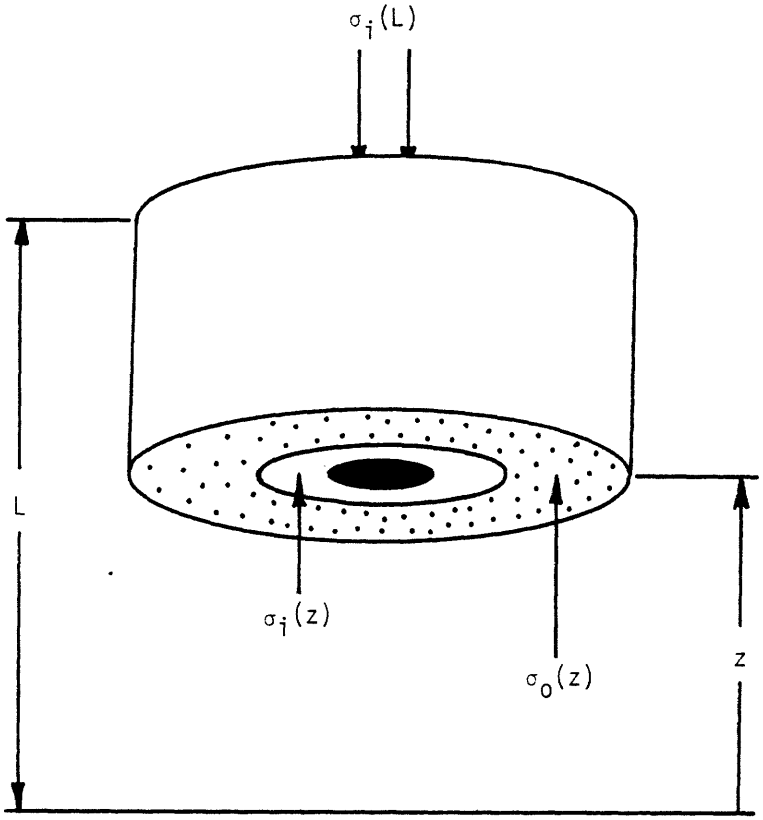

Case 1

This equation is solved, and evaluated at z = L to yield the insertion force, F_1:

$$F_1 = \left(\frac{\delta}{b}\right) \frac{A_i E_i}{\nu_i} \left[\frac{e^{kL} - 1}{\frac{\nu_o A_i E_i}{\nu_i A_o E_o} e^{kL} + 1} \right] \tag{2.20}$$

where

$$kL = \left(\frac{\mu L}{b}\right)(\pi b^2 E_e)\left(\frac{\nu_i}{E_i A_i} + \frac{\nu_o}{E_o A_o} \right) \tag{2.21}$$

For identical materials,

$$kL = \nu\left(\frac{\mu L}{b}\right) \tag{2.22}$$

By changing the appropriate algebraic signs in Eq. (2.20), the withdrawal force in loading Case #3 is given by:

$$F_3 = \left(\frac{\delta}{b}\right) \frac{A_i E_i}{\nu_i} \left[\frac{1 - e^{-kL}}{1 + \frac{\nu_o A_i E_i}{\nu_i A_o E_o} e^{-kL}} \right] \tag{2.23}$$

For kL < 0.5, these equations may be expanded into the approximations

$$F_1 = \mu L(\pi \delta E_e)\left(1 + \frac{kL}{2} \left[\frac{1 - \frac{\nu_o A_i E_i}{\nu_i A_o E_o}}{1 + \frac{\nu_o A_i E_i}{\nu_i A_o E_o}} \right] \right) \tag{2.24}$$

$$F_3 = \mu L(\pi \delta E_e)\left(1 - \frac{kL}{2} \left[\frac{1 - \frac{\nu_o A_i E_i}{\nu_i A_o E_o}}{1 + \frac{\nu_o A_i E_i}{\nu_i A_o E_o}} \right] \right) \tag{2.25}$$

If the ratio EA/ν is the same for each cylinder, these approximate equations reduce to Eq. (2.12) where the Poisson effect was neglected.

CASE #2

In this loading situation, the inner cylinder is put in compression, and the outer cylinder in tension from the application of the insertion force, F_2. Figure 2.2, Eqs. (2.16 and 2.18) are still valid in this case. However, if a section through both cylinders is taken, Figure 2.4, stress equilibrium implies

$$\sigma_o(z) = \frac{-A_i}{A_o} \sigma_i(z) \tag{2.26}$$

Substitution Eqs. (2.8, 2.16 and 2.26) into Eq. (2.18), the differential equation for $\sigma_i(z)$ is obtained:

$$\left(\frac{b^2 - a^2}{\mu b E_e}\right) \frac{d\sigma_i(z)}{dz} - \left(\frac{\nu_i}{E_i} + \frac{\nu_o A_i}{E_o A_o}\right)\sigma_i(z) - \frac{\delta}{b} = 0 \tag{2.27}$$

Solving this equation, and evaluating $\sigma_i(z)$ at $z = L$,

$$F_2 = \frac{\left(\frac{\delta}{b}\right)}{\frac{\nu_i}{E_i A_i} + \frac{\nu_o}{E_o A_o}} (e^{kL} - 1) \tag{2.28}$$

where kL was defined by Eq. (2.21). The withdrawal force, F_3, is found by changing the appropriate algebraic signs in Eq. (2.28):

$$F_4 = \frac{\left(\frac{\delta}{b}\right)}{\frac{\nu_i}{E_i A_i} + \frac{\nu_o}{E_o A_o}} (1 - e^{-kL}) \tag{2.28}$$

These equations for insertion and withdrawal force, including approximations, are summarized in Tables 2.1 and 2.2.

The magnitude of the Poisson effect may be examined by considering the ratio

$$\frac{F \text{ (including Poisson effect)}}{F \text{ (by constant pressure assumption)}}.$$

Figure 2.4

Forces acting on inner and outer cylinders.

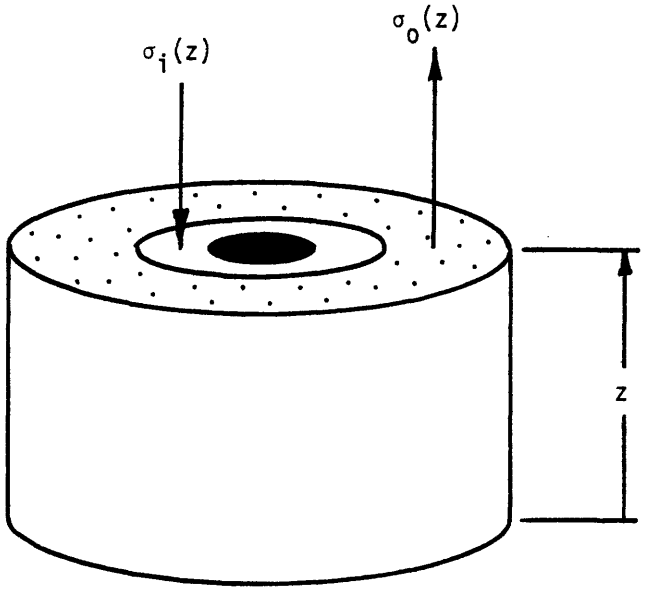

Case 2

Table 2.1

Insertion force equations including Poisson effect.

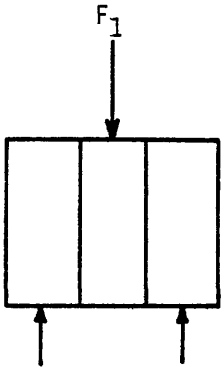

$$F_1 = \left(\frac{\delta}{b}\right)\frac{A_i E_i}{\nu_i}\left[\frac{e^{kL}-1}{\frac{\nu_o A_i E_i}{\nu_i A_o E_o}\,e^{kL}+1}\right]$$

$$F_1 \simeq \mu L(\pi\delta E_e)\left(1+\frac{kL}{2}\left[\frac{1-\frac{\nu_o A_i E_i}{\nu_i A_o E_o}}{1+\frac{\nu_o A_i E_i}{\nu_i A_o E_o}}\right]\right)$$

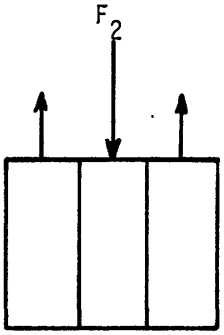

$$F_2 = \frac{\left(\frac{\delta}{b}\right)}{\frac{\nu_i}{E_i A_i}+\frac{\nu_o}{E_o A_o}}\left(e^{kL}-1\right)$$

$$F_2 \simeq \mu L(\pi\delta E_e)\left(1+\frac{kL}{2}\right)$$

where

$$kL = \left(\frac{\mu L}{b}\right)(\pi b^2 E_e)\left(\frac{\nu_i}{E_i A_i}+\frac{\nu_o}{E_o A_o}\right)$$

For identical materials,

$$kL = \nu\left(\frac{\mu L}{b}\right)$$

Table 2.2

Withdrawal force equations including Poisson effect.

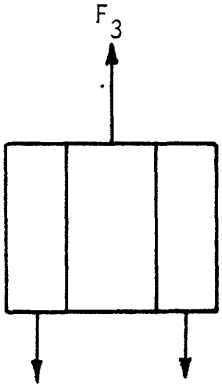

$$F_3 = \left(\frac{\delta}{b}\right)\frac{A_i E_i}{\nu_i}\left[\frac{1 - e^{-kL}}{1 + \frac{\nu_o A_i E_i}{\nu_i A_o E_o}\, e^{-kL}}\right]$$

$$F_3 \simeq \mu L(\pi\delta E_e)\left(1 - \frac{kL}{2}\left[\frac{1 - \frac{\nu_o A_i E_i}{\nu_i A_o E_o}}{1 + \frac{\nu_o A_i E_i}{\nu_i A_o E_o}}\right]\right)$$

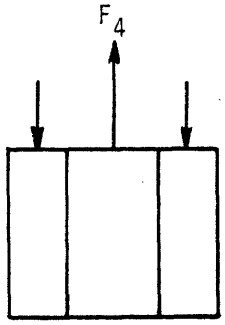

$$F_4 = \frac{\left(\frac{\delta}{b}\right)}{\frac{\nu_i}{E_i A_i} + \frac{\nu_o}{E_o A_o}}\,(1 - e^{-kL})$$

$$F_4 \simeq \mu L(\pi\delta E_e)\left(1 - \frac{kL}{2}\right)$$

where

$$kL = \left(\frac{\mu L}{b}\right)(\pi b^2 E_e)\left(\frac{\nu_i}{E_i A_i} + \frac{\nu_o}{E_o A_o}\right)$$

For identical materials,

$$kL = \nu\left(\frac{\mu L}{b}\right)$$

This ratio is plotted in Figure 2.5 for cylinders of identical material properties. If the contact length to interference diameter ratio, L/2b, is two, for example, the Poisson effect is bounded by a maximum force increase of 13% (insertion by method 2) and a maximum force decrease of 11% (withdrawal method 4), where Poisson's ratio = 0.3 and the friction coefficient = 0.2.

Thus, for interference fits having low length to diameter ratios, the Poisson effect may be neglected in comparison with the uncertainties regarding the friction coefficient.

2.3 The Effect of Pressure Concentrations

The previous analysis assumed that with no axial stresses, the interference pressure would be the same at all points of contact. This is a valid assumption for fully engaged cylinders of equal length. However, in every other case, there will be a stress concentration where a shaft enters a hole and where a shaft ends in a hole. Far from these points of discontinuity, if the contact length is sufficiently long, the interference pressure approaches the constant value given by Eq. (2.7). Thus, in determining insertion and withdrawal forces, the equal length cylinder assumption would become increasingly valid as the contact length to interference diameter ratio increases.

Previous studies have focused primarily on finding the contact stresses resulting from mounting a short frictionless cylindrical collar onto a solid shaft of infinite length. Rankin[13] measured the deformation of a shaft upon which a short hub was mounted and then determined what equivalent uniform band of pressure would be required to account for these measured radial displacements.

More recent studies[8-11] have used finite element methods to determine the actual pressure distribution for collars of various lengths and thicknesses. The general trend for cylinders of identical material is shown in Figure 2.6.

The interference fit problem studied by Rankin has been analyzed using a finite element computer program[10]. The dimensions are shown in Figure 2.7, while the pressure distribution is plotted in Figure 2.8.

Figure 2.5

Poisson effect of axial stresses

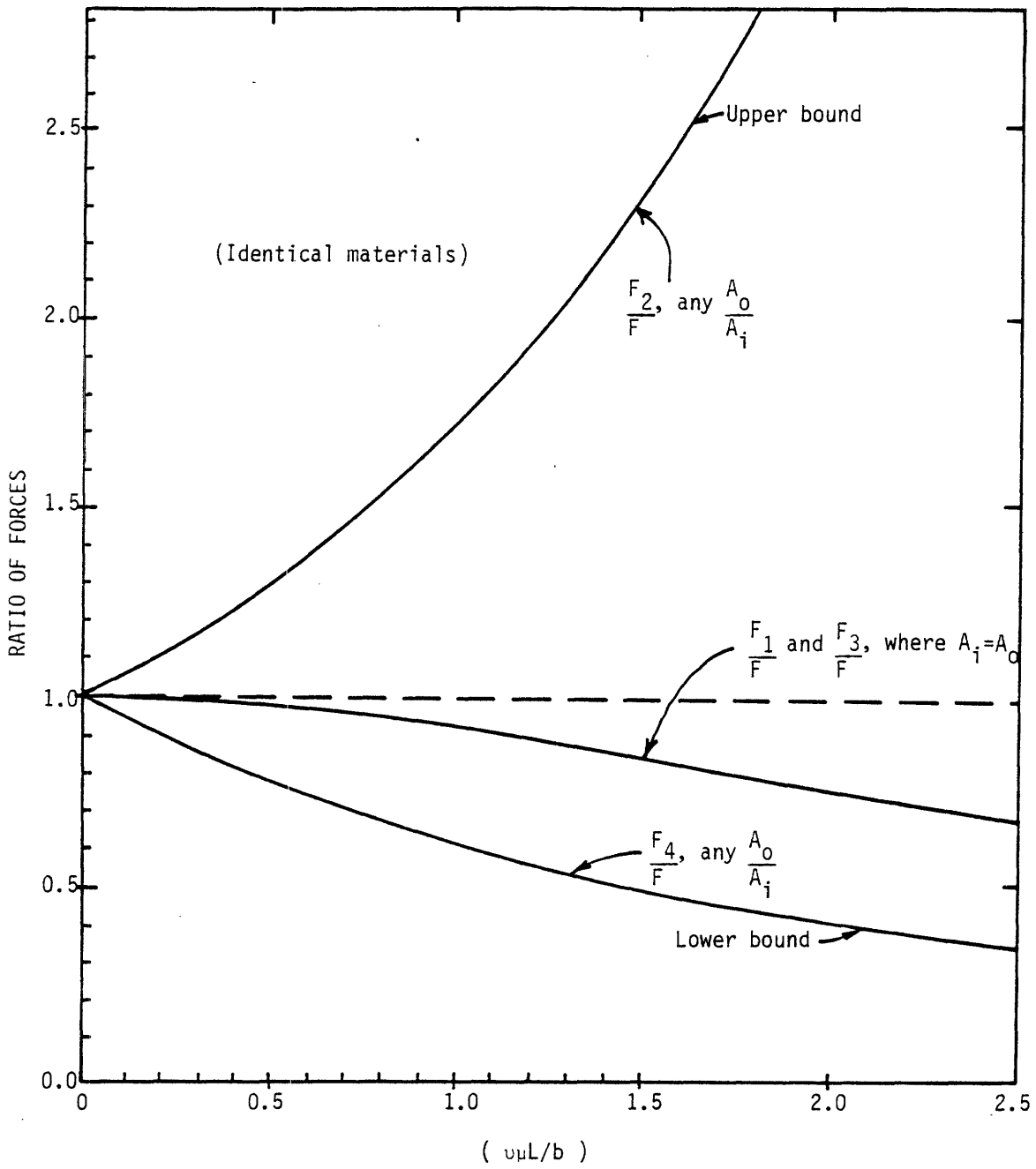

Figure 2.6

Interference pressure for a short collar

fit onto a long shaft.

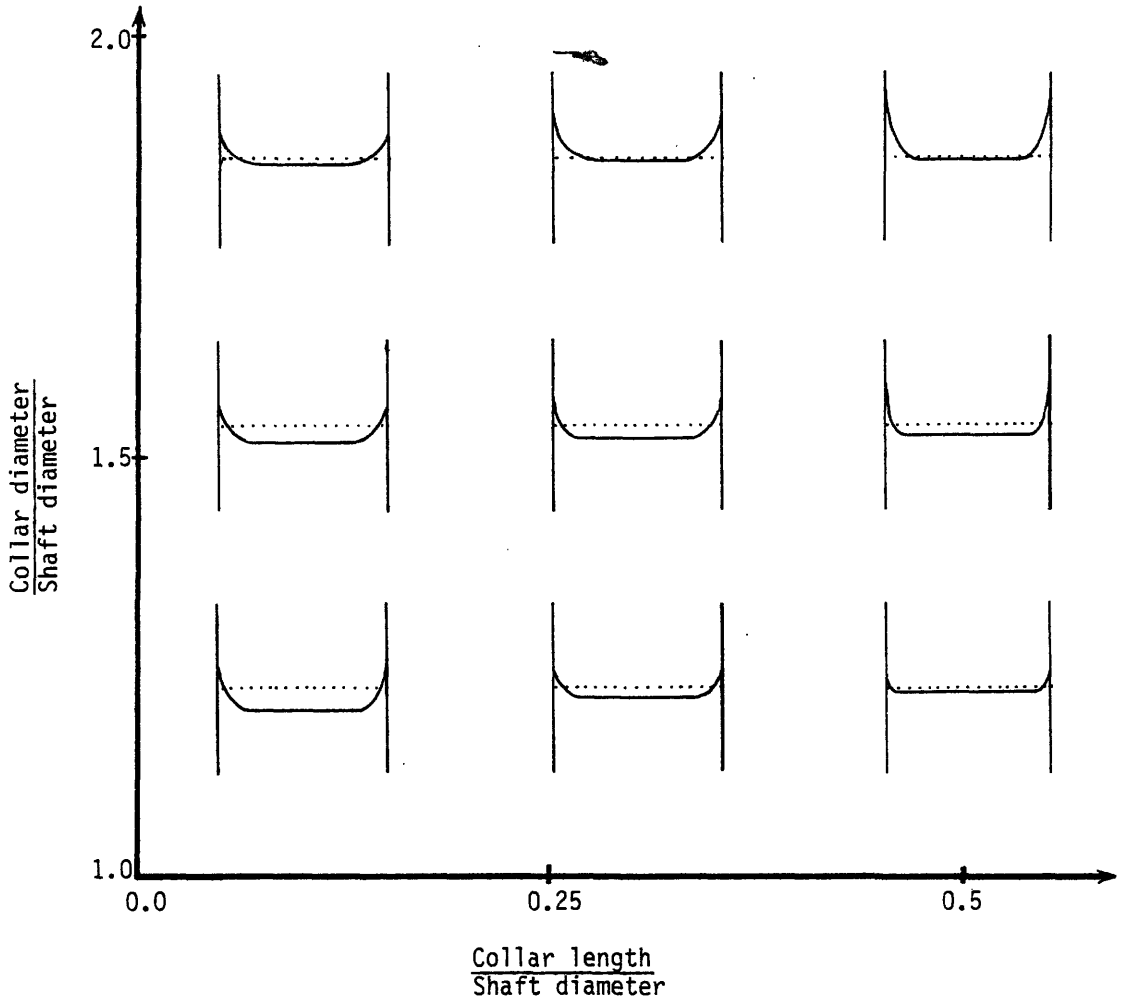

Calculated pressure based on Eq. (2.7)

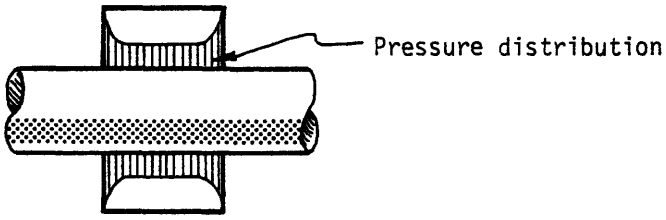

Figure 2.7

Interference fit studied by Rankin.

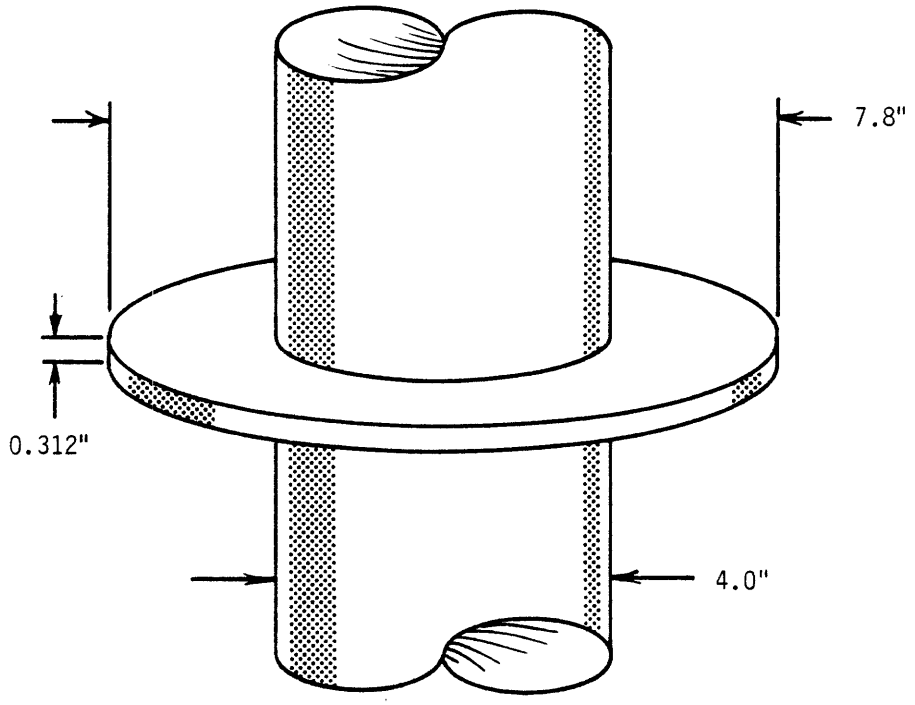

Interference = 0.0043 in.

Steel shaft and collar

Figure 2.8

Comparison of stress distribution

based on finite-element analysis and approximate analysis.

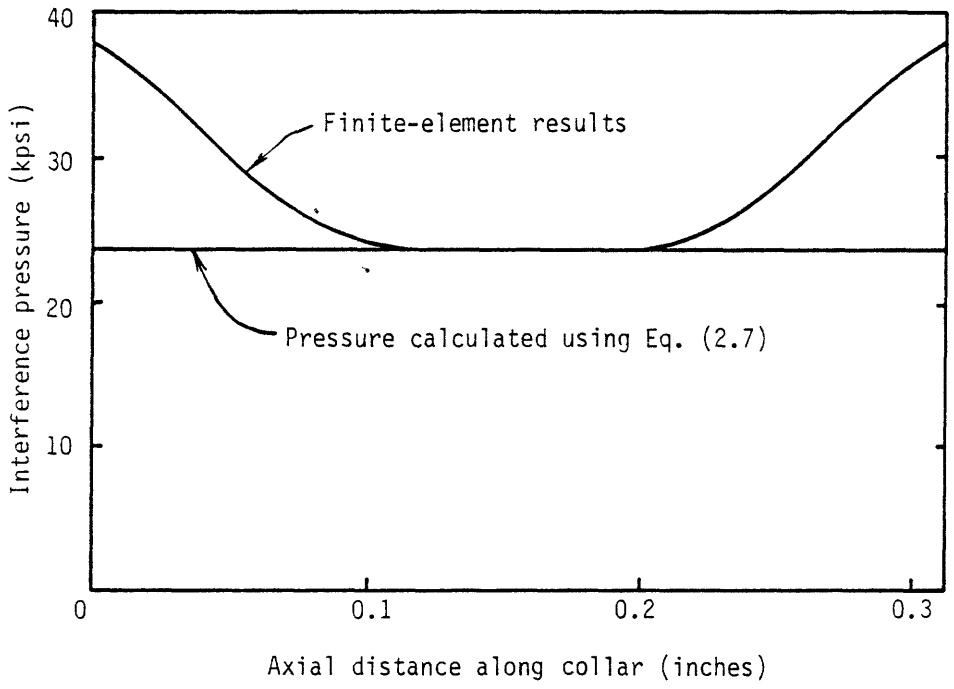

The insertion force is found by measuring the area under the curve:

$$F_I = \mu(2\pi b) \int p\,dz \qquad (2.29)$$

Using the constant pressure assumption, Eq. (2.12), one predicts an insertion force 16% less than if Figure 2.8 and Eq. (2.29) are used (axial stress Poisson effect is negligable). Thus, even in this case where there is a considerable deviation from constant pressure, the predicted insertion force is within the margin of uncertainty in the coefficient of friction. Furthermore, since the contact length to interference diameter ratio (L/2b) was 0.078, extremely small, and accuracy improves as L/2b increases, this study indicates that in determining insertion and withdrawal forces, end effects may be neglected in practical applications.

3.0 IMPACT LOADING

This section investigates the behavior of interference fits subject to the forces of impact. The emphasis here will be on the assembly of interference fits by impact methods. The same concepts may be used in evaluating the impact absorbing capability of fits subject to service loads which are impulsive in nature.

Throughout the analysis, the following assumptions are made:

1) The interference pressure is constant along the length of contact
2) Relative sliding between the parts is governed by Coulomb friction
3) Axial stresses change in the axial direction only

3.1 Axial Stress Distributions in the Loading Process

Given the above assumptions, an interference fit may be modeled as two sets of spring-block chains coupled by Coulomb friction, as shown in Figure 3.1. Quasi-static loading is considered, so that inertia effects may be ignored.

When the static insertion force, F_I, is applied (given by Eq. (2.12)), the axial stress in each cylinder decreases linearly with depth, as shown in Figure 3.2. If the insertion force is now removed from the loaded cylinders, residual axial stresses will result. In addition, slippage between the parts will occur over certain portions of the contact area.

First, consider the removal of the insertion force assuming there is infinite friction between the parts (no slippage). The forces acting on a section of incremental thickness during initial loading and final equilibrium are shown in Figure 3.3. In order to satisfy the constraint

$$\sigma_i A_i + \sigma_i A_o = 0 \tag{3.1}$$

at all depths, the cylinders undergo uniform expansion until the resulting elongation of each incremental section is given by:

$$e = \frac{F_I}{E_i A_i + E_o A_o}\, dz \tag{3.2}$$

Figure 3.1

Interference fit continuum model.

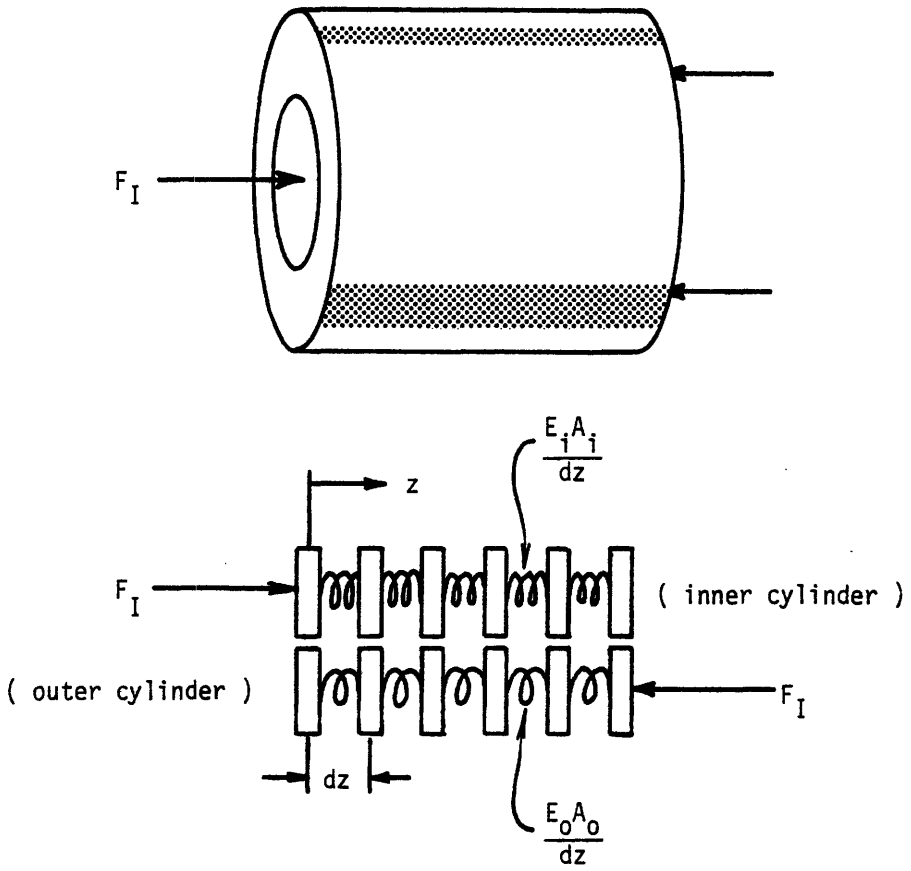

Friction force between elements $\leq F_I \frac{dz}{L}$

where E = modulus of elasticity

A = cross-sectional area

F_I = static insertion force

L = length of contact

Figure 3.2

Axial stresses in a loaded interference fit.

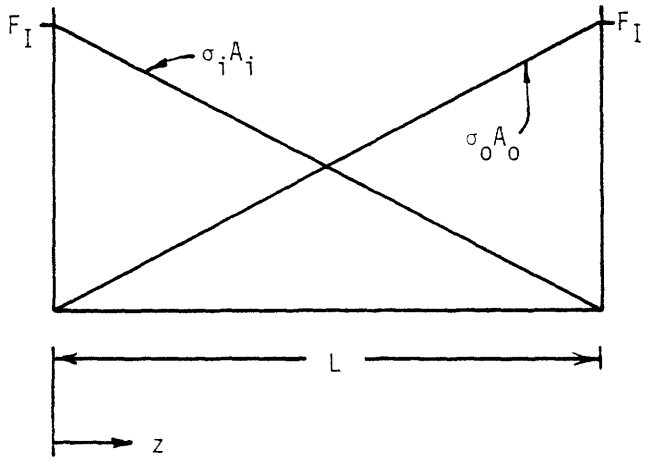

Figure 3.3

Unloading of a fit with infinite friction

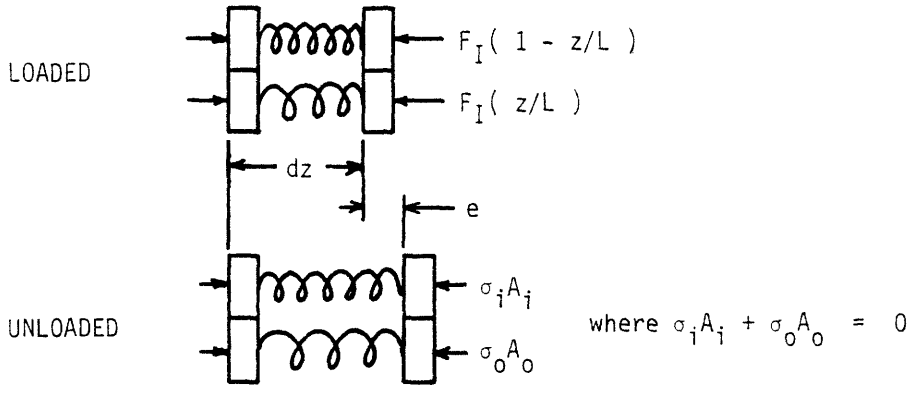

Thus, the axial stress in each cylinder is reduced by a constant amount:

$$\Delta\sigma_i = \frac{E_i A_i}{E_i A_i + E_o A_o} \frac{F_I}{A_i} \tag{3.3}$$

$$\Delta\sigma_o = \frac{E_o A_o}{E_i A_i + E_o A_o} \frac{F_I}{A_o} \tag{3.4}$$

The resulting stress distribution with the insertion force removed (infinite friction) is shown in Figure 3.4. At all depths, where one cylinder is in compression, the other is in a corresponding state of tension.

At this point, slippage has not been allowed. This requirement implies that the ends of the cylinders are held together with infinite friction, while all interior points exert the maximum friction, $F_I dz/L$. The final stress equilibrium is found by allowing successive elements to slip, starting at the endpoints of the cylinders. This process is shown in Figure 3.5. The resulting residual axial stresses in the unloaded interference fit are shown in Figure 3.6. The ratio of the axial stiffnesses of the two cylinders, $E_i A_i / E_o A_o$, determines how the axial stresses will change, and where slipping will occur.

The axial stress distribution for an arbitrary axial load, F, may be determined by the same method as used above (this is shown in Figure 3.7). The axial load uniquely determines the stress distribution, whether the fit is being loaded or unloaded.

3.2 Energy Absorbed in Loading

A certain amount of energy (work) must be supplied to bring an interference fit from an unloaded to a loaded condition. Part of this work is stored in the cylinders in the form of elastic strain energy which is recoverable. The remainder is lost in heat, produced at the areas of slippage through frictional sliding.

Consider an interference fit initially loaded by an arbitrary axial force, F. The energy required to increase the load up to the insertion force, F_I, will be calculated.

Figure 3.4

Residual axial stresses in an unloaded interference fit with infinite friction.

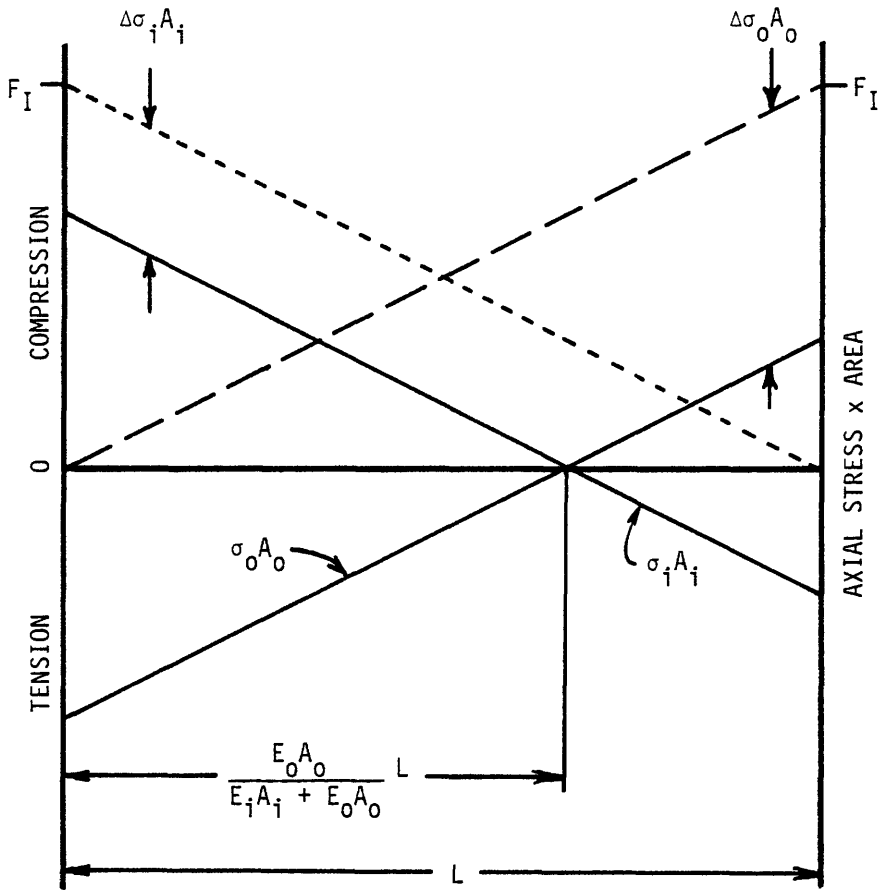

Figure 3.5

Allowing slippage to occur between the cylinders

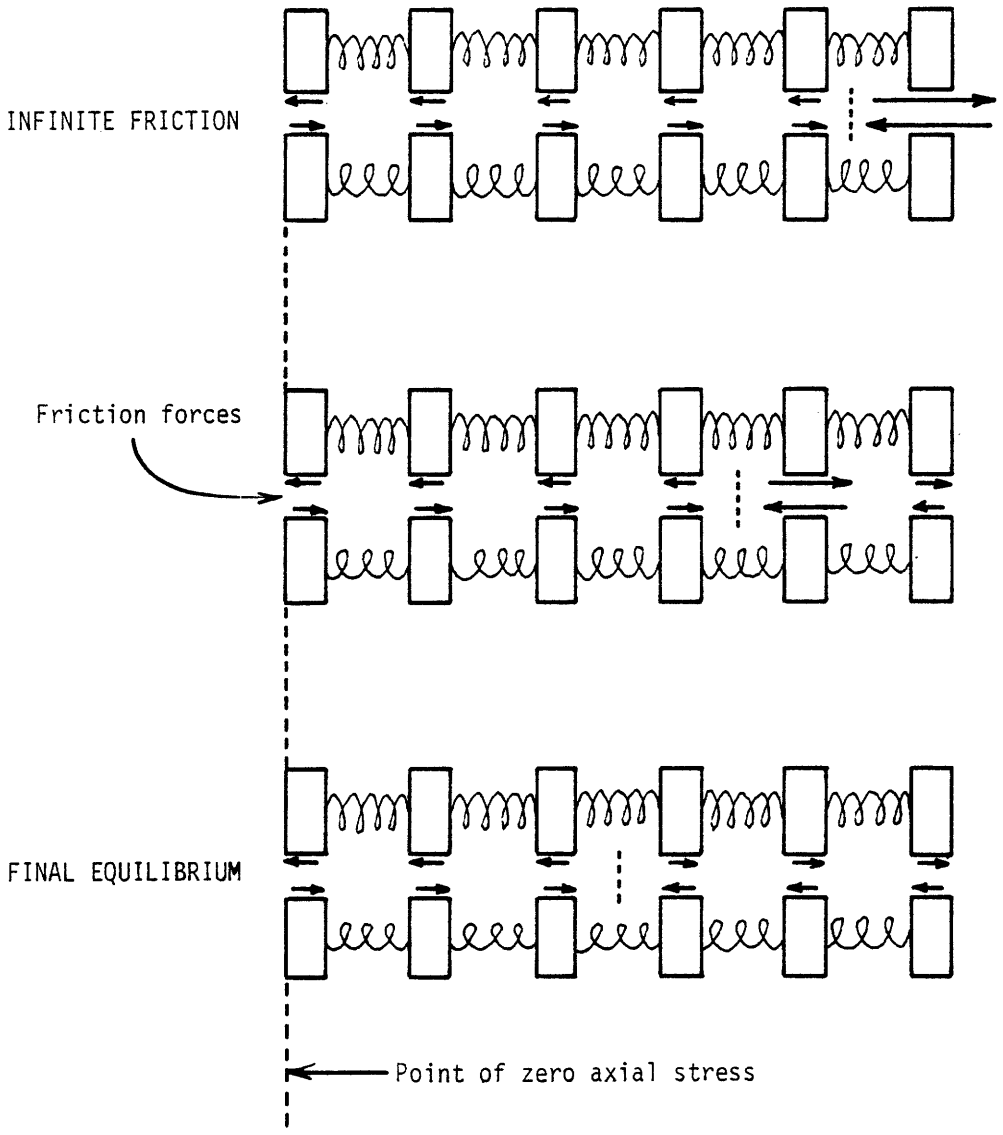

Figure 3.6

Residual axial stresses in an unloaded interference fit, final equilibrium.

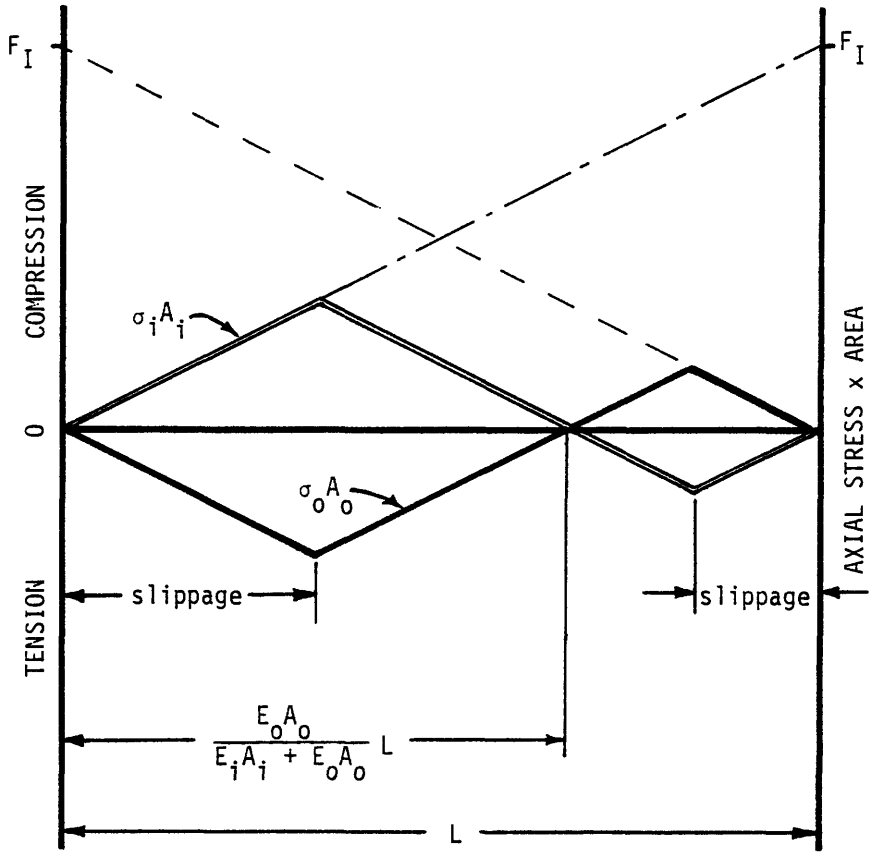

Figure 3.7

Axial stress distribution for an arbitrary axial load

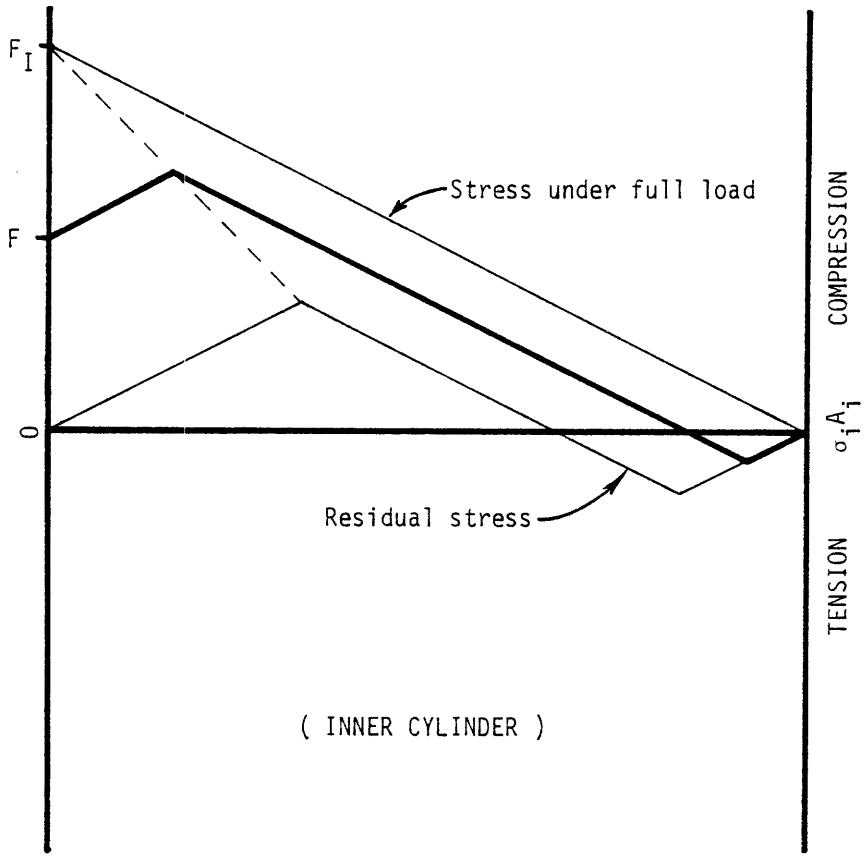

REQUIRED STRAIN ENERGY

If $\sigma_{F_I}(z)$ is the axial stress function resulting from the application of the insertion force, F_I, and $\sigma_F(z)$ corresponds to an arbitrary load F, where $F < F_I$, the difference in strain energy is given by:

$$U_s = A/2E \int_0^L (\sigma_{F_I}(z)^2 - \sigma_F(z)^2) \, dz \tag{3.5}$$

The axial stress functions $\sigma_{F_I}(z)$ and $\sigma_F(z)$ for the inner cylinder are specified in Figure 3.8. A straightforward but tedious integration of Eq. (3.5) using these stress functions yields an expression for the strain energy absorbed by the inner cylinder. By replacing E_iA_i by E_oA_o, and vice versa, in this equation, the energy absorbed by the outer cylinder is found. The total strain energy absorbed by both cylinders is then given by:

$$U_s = \frac{F_I^2 L}{8}\left(1 - \frac{F}{F_I}\right)\left[\left(\frac{1}{E_iA_i} + \frac{1}{E_oA_o} - \frac{3}{E_iA_i + E_oA_o}\right)\left(\frac{F}{F_I}\right)^2 + \left(\frac{4}{E_iA_i + E_oA_o}\right)\frac{F}{F_I} + \frac{1}{E_iA_i} + \frac{1}{E_oA_o} + \frac{1}{E_iA_i + E_oA_o}\right] \tag{3.6}$$

The strain energy requirement to bring the interference fit from an unloaded (F=0) to a fully loaded state is then:

$$U_s = \frac{F_I^2 L}{8}\left(\frac{1}{E_iA_i} + \frac{1}{E_oA_o} + \frac{1}{E_iA_i + E_oA_o}\right) \tag{3.7}$$

REQUIRED FRICTIONAL WORK:

If the load on the interference fit is reduced from F_I to F, the resulting axial stress functions corresponding to infinite friction (no slip) may be found as in section 3.1. When the cylinders are now allowed to slip, in reaching final

Figure 3.8

Axial stress functions for the inner cylinder

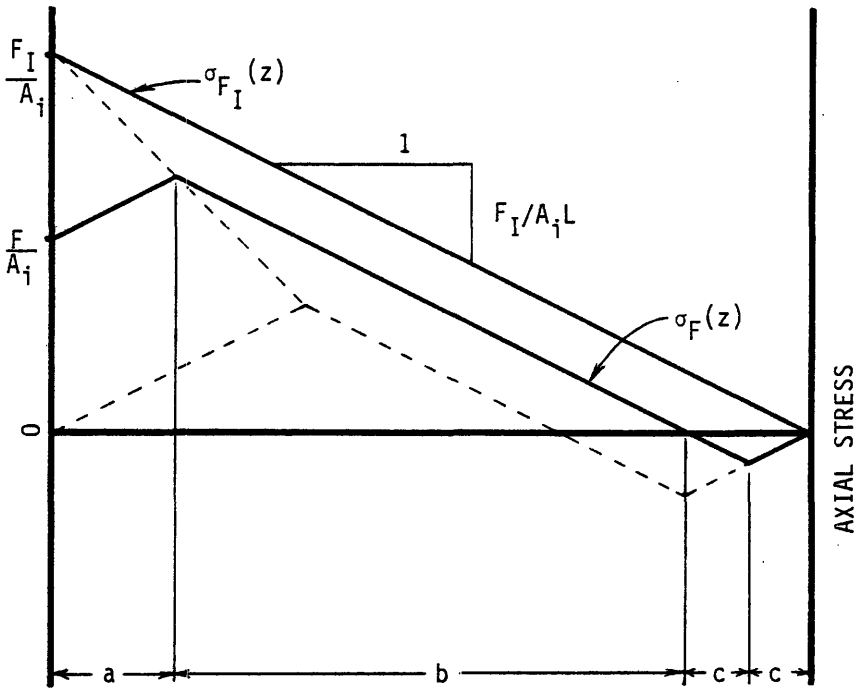

$$a = \frac{1}{2}\frac{E_oA_o}{E_iA_i + E_oA_o}\left(1 - \frac{F}{F_I}\right)L$$

$$b = L - \left(1 + \frac{2E_iA_i}{E_oA_o}\right)a$$

$$c = \frac{E_iA_i}{E_oA_o}a$$

equilibrium, the stress functions will change only in the places where slipping occurs. The changes in the axial stress functions may be used to determine the relative displacement of each cylinder. The energy lost in frictional sliding is given by:

$$U_f = \int_0^L \frac{F_I}{L} \mid u_i(z) - u_o(z) \mid dz \tag{3.8}$$

where $u_i(z)$ = displacement of inner cylinder when allowed to slip

$u_o(z)$ = displacement of outer cylinder when allowed to slip

The stress functions corresponding to infinite friction, and final equilibrium are shown in Figure 3.9. When the cylinders are allowed to slip, the axial stress in each cylinder is changed by the following amount:

$$\Delta\sigma(z) = \frac{2F_I}{A\,L}\, z \tag{3.9}$$

where the variable z is defined in Figure 3.9. The resulting displacement is given by:

$$u(z) = 1/E \int_0^z \Delta\sigma(z)\, dz \tag{3.10}$$

Substituting in Eq. (3.9), and integrating, the displacement of each cylinder when allowed to slip is found:

$$\mid u_i(z) \mid = \frac{F_I\, z^2}{E_i A_i L} \tag{3.11}$$

$$\mid u_o(z) \mid = \frac{F_I\, z^2}{E_o A_o L} \tag{3.12}$$

Evaluating Eq. (3.8) at the two areas of slippage, using Eqs. (3.11) and (3.12), the amount of energy lost in frictional sliding is given by:

Figure 3.9

Change in axial stress when cylinders are allowed to slip

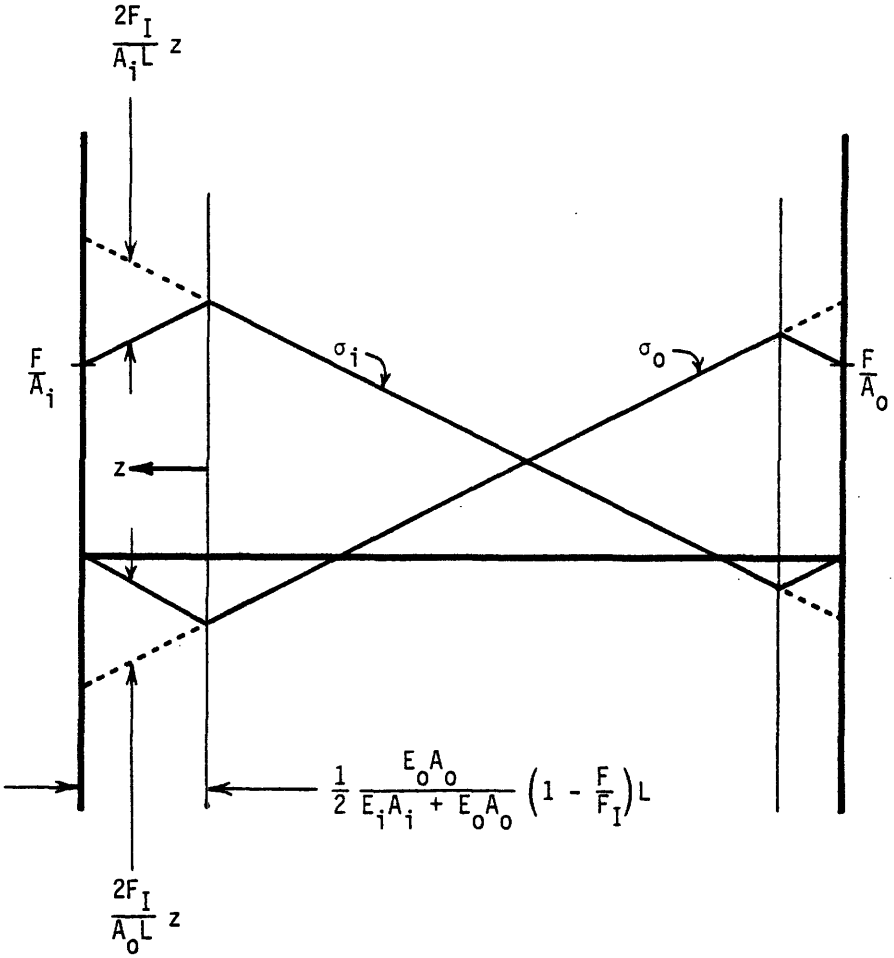

$$U_f = \frac{F_I^2 L}{24}\left(1 - \frac{F}{F_I}\right)^3\left(\frac{1}{E_iA_i} + \frac{1}{E_oA_o} - \frac{3}{E_iA_i + E_oA_o}\right) \tag{3.13}$$

The total amount of energy required to increase the load on an interference fit from an arbitrary force, F, to the insertion force, F_I, is given by $U_s + U_f$, and will be called the threshold energy, U_o.

$$U_o = \frac{F_I^2 L}{6}\left(1 - \frac{F}{F_I}\right)\left[\left(\frac{1}{E_iA_i} + \frac{1}{E_oA_o} - \frac{3}{E_iA_i + E_oA_o}\right)\left(\frac{F}{F_I}\right)^2 + \frac{1}{2}\left(\frac{9}{E_iA_i + E_oA_o} - \frac{1}{E_iA_i} - \frac{1}{E_oA_o}\right)\frac{F}{F_I} + \frac{1}{E_iA_i} + \frac{1}{E_oA_o}\right] \tag{3.14}$$

The threshold energy plotted as a function of preload force, F, is shown in Figure 3.10. When the interference fit is initially unloaded (F=0), the threshold energy is given by:

$$U_o = \frac{F_I^2 L}{6}\left(\frac{1}{E_iA_i} + \frac{1}{E_oA_o}\right) \tag{3.15}$$

The fraction of the threshold energy which is frictional work is shown in Figure 3.11.

3.3 Quasi-static Impact Model

An approximate analysis of the response of an interference fit subjected to an applied impact load can be made using the threshold energy equations derived above. The mass of the interference fit is neglected, allowing the impact to be modeled as time independent, or quasi-static loading. This analysis will determine what movement (insertion) will occur when an interference fit receives a blow from a hammer.

Consider a mass, M, having a kinetic energy, $\frac{1}{2}MV^2$, at the instant before

Figure 3.10

The effect of preload force on threshold energy

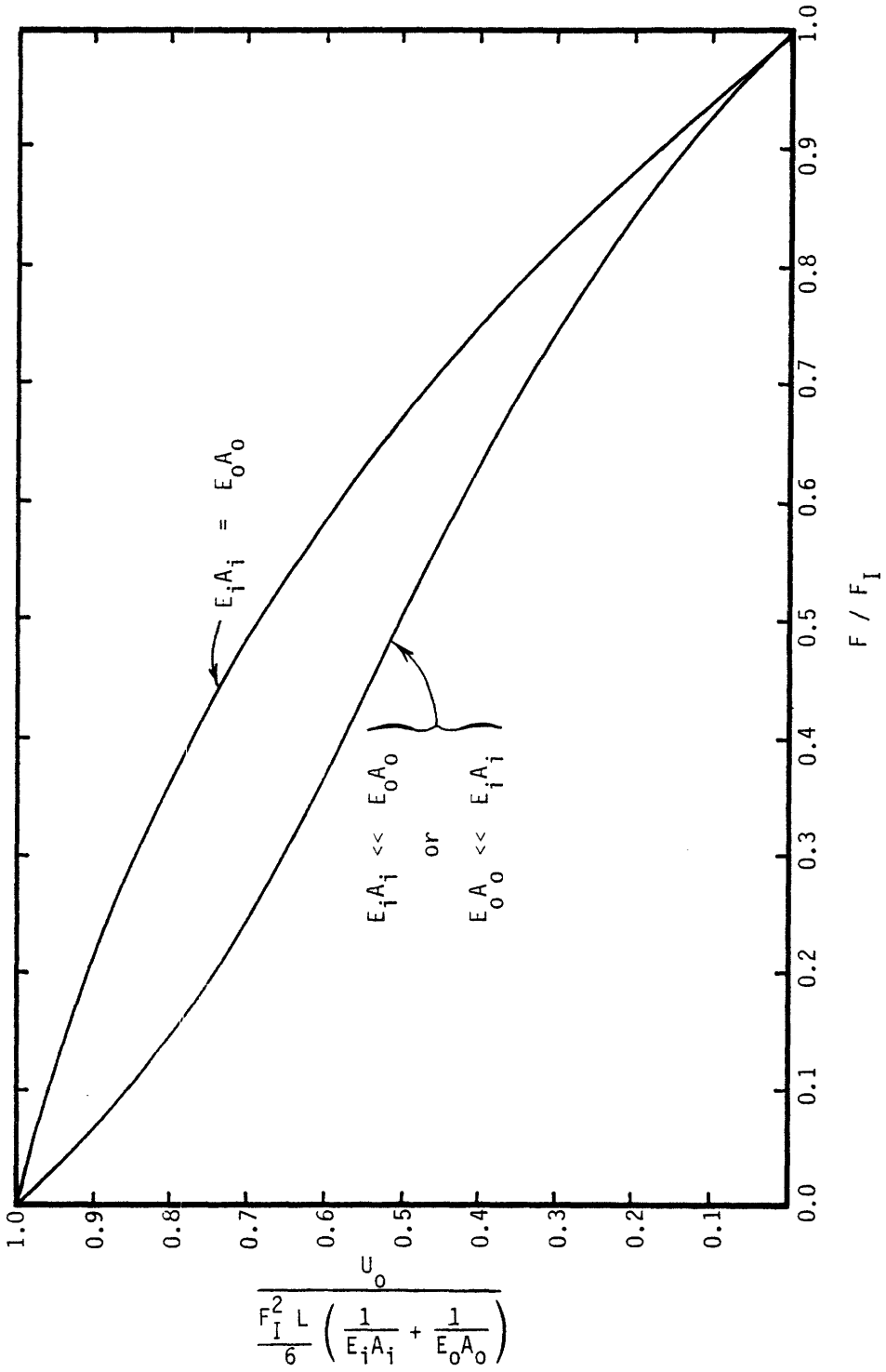

Figure 3.11

Percent of the threshold energy which is frictional work

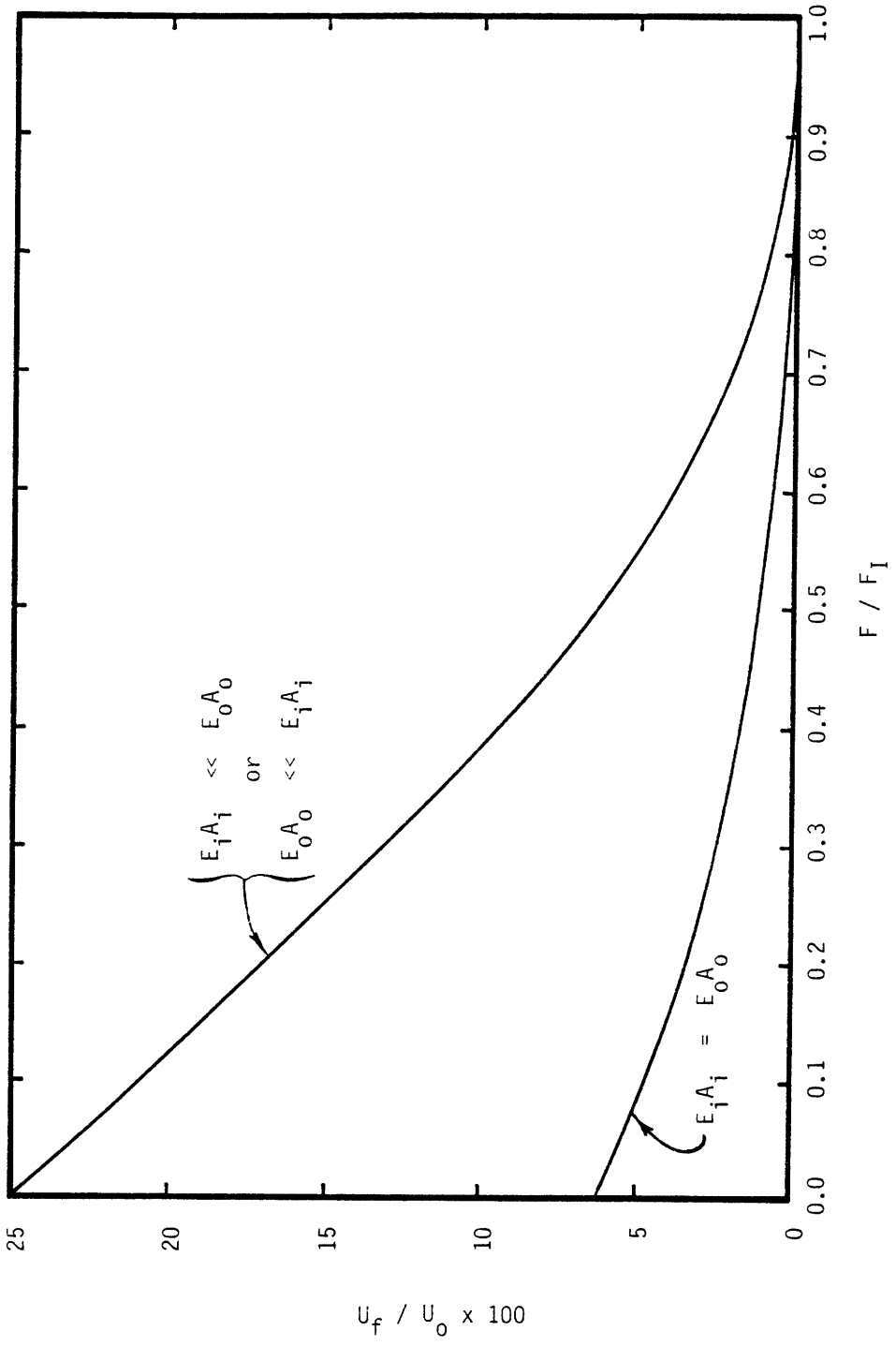

striking the interference fit. If this kinetic energy is less than the threshold energy, U_o, no insertion will take place. If, however, the kinetic energy is greater than the threshold, conservation of energy implies:

$$F_I \Delta L = U_H - U_o \tag{3.16}$$

where $U_H = \frac{1}{2}MV^2$ = kinetic energy of hammer

F_I = static insertion force

ΔL = motion per hit

The threshold energy given by Eq. (3.15) is for concentric cylinders of equal length. If the inner cylinder (shaft) protrudes a distance L_i, the the equation for threshold energy with no preload becomes:

$$U_o = F_I^2 \left[\frac{L}{6}\left(\frac{1}{E_i A_i} + \frac{1}{E_o A_o}\right) + \frac{L_i}{2}\left(\frac{1}{E_i A_i}\right) \right] \tag{3.17}$$

If the interference fit has a preload force, F, applied to it as the impact takes place, conservation of energy implies:

$$(F_I - F) \Delta L = U_H - U_o \tag{3.18}$$

where the threshold energy includes the effect of the preload force, as given by Eq. (3.14).

Since the mass of the interference fit was neglected in this analysis, one would expect these results to become increasingly accurate as the mass of the striking object becomes much larger than that of the interference fit.

3.4 Impact Dynamics

A more exact analysis of impact takes into account inertia effects and so treats the variation of stress and strain at each point in the interference fit as a function of time. Due to the presence of Coulomb friction, which acts at the

interface between the parts, the governing coupled partial differential equations are nonlinear. The problem is highly complex because of the transmission and reflection of elastic waves at the frictional boundary, and wave reflection at free surfaces. In addition, the applied force must either be completely prescribed, or the striking mass must be assumed to be rigid.

The special case of a stress pulse applied to an elastic rod of infinite length bounded by Coulomb friction is the only problem for which an exact analytic solution has been obtained[14,15]. This is of very limited usefulness, however, since the transmission of elastic waves through the frictional boundary and into the outer member has been neglected. A useful method of analysis may be an equivalent linearization method[16] in which the Coulomb friction is modeled as a combination of linear terms such that the mean square difference between the steady state solutions is minimized.

4.0 IMPACT EXPERIMENTS

Two experiments were performed to test the validity of the quasi-static analysis presented in section 3.3. In each case, a solid shaft was pressed into a collar of shorter length so that the shaft protruded from the top. The interference fits were placed on the bed of a milling machine in order to provide a relatively stiff surface in comparison with the compliance of the fits themselves. A hammer was dropped onto the interference fits from various heights, and the resulting insertion per hit was measured.

The hammer was dropped at a given height from 10 to 75 times to produce a net insertion of about 0.02 to 0.05 inches. This was measured by placing a depth micrometer on a stable reference surface, with the tip touching the top of the protruding shaft. After about 0.1 inches of total insertion was produced, the fit was pressed back into its original location, and the static insertion force was measured using a Dillon force gage. In both cases, the static insertion force varied about 10 percent throughout the experiment, while an overall decrease was not observed as the number of insertion/withdrawal cycles increased.

In the first experiment, the insertion force was approximately 2200 lbs. and the hammer weight was 3.2 lbs. In the second, the insertion force was about 720 lbs. and the hammer weighed 8 oz.

The dimensions and calculated threshold energy using Eq. (3.17) for each is listed in Table 4.1.

The height from which the hammer was dropped, H, and the resulting insertion per hit, ΔL, were made dimensionless by using Eq. (3.16) in dimensionless form:

$$\frac{F_I}{U_o} \Delta L = \frac{W}{U_o} H - 1 \qquad (4.1)$$

The results of the two experiments are shown in Figure 4.1. No insertion was observed until the energy of the hammer was about four times the threshold energy. The heavy 3 lb. hammer matched the theoretical prediction for energies

Table 4.1

Specifications of interference fits used in experiments

First experiment:

Materials: both hardened ground steel, $E = 30 \times 10^6$ psi

$L = 0.750$ in.

$2b = 0.375$ in.

$2c = 0.813$ in.

$L_i = 0.60$ in.

$A_i = 0.110$ in.^{2}

$A_o = 0.408$ in.^{2}

$F_I = 2200$ lbs.

$W = 3.2$ lbs.

$U_o = 0.672$ in-lbs.

Second experiment:

Materials: both mild steel, $E = 30 \times 10^6$ psi

$L = 0.625$ in.

$2b = 0.440$ in.

$2c = 0.970$ in.

$L_i = 0.98$ in.

$Ai = 0.152$ in.^{2}

$A_o = 0.587$ in.^{2}

$F_I = 720$ lbs.

$W = 0.5$ lbs.

$U_0 = 0.071$ in-lbs.

Figure 4.1

Results of impact experiments.

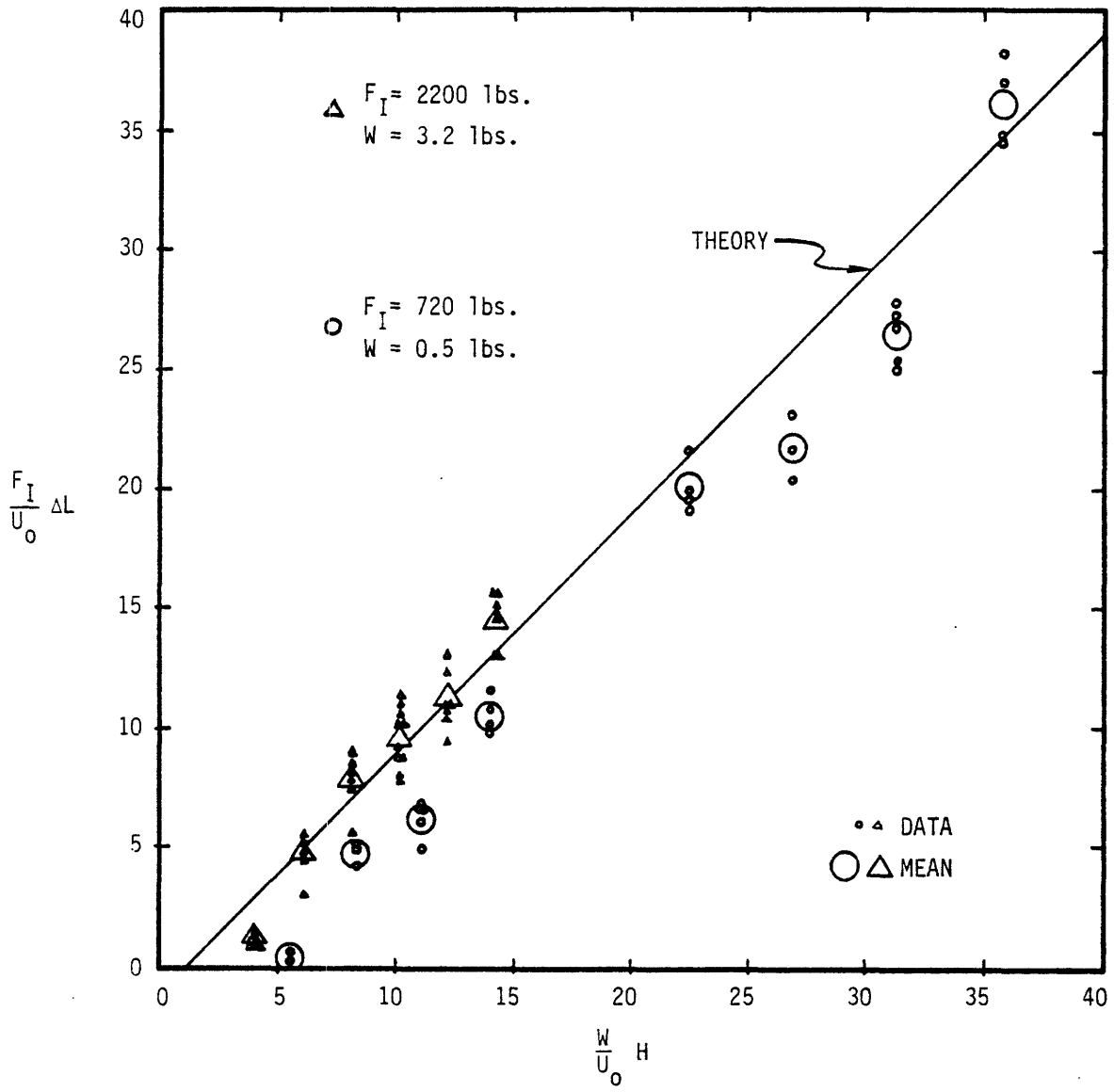

greater than about 7 times the threshold energy. The relatively light 8 oz. hammer was not as effective as the theory predicted until the supplied energy was greater than about 35 times the threshold energy. This was expected since the dynamics of the situation was ignored in the analysis and becomes important when the weight of the hammer becomes small compared with the weight of the parts.

5.0 CONCLUSIONS AND RECOMMENDATIONS

In many cases, the interference fit has axial symmetry, and so the analysis of concentric cylinders is a good approximation to the actual geometry involved. However, parts of non cylindrical geometry often occur, such as when pins or bushings are pressed into housings. The applicability of the cylindrical analysis to these cases should be explored further.

It has been found that the holding power of an interference fit can be increased if the interference is chosen large enough to cause the stress in the parts to exceed the elastic limit. Thus it is not uncommon for a fit to be designed so that the parts yield. If the elastic analysis is used in this case, the calculated pressure, and so the insertion and withdrawal forces, wil be overestimated. The analysis of plastic flow in pressurized cylinders must be applied to this situation for a more accurate description.

The inclusion of the Poisson effect eliminates one of the factors of uncertainty regarding the calculation of insertion and holding forces. Experiments should be undertaken to see how accurate the theoretical predictions are.

The primary source of error in both the Poisson and the energy analyses is the assumption that axial stresses are uniform on any circular cross-section of a cylinder. For the inner member, or shaft, this is a valid assumption. However, if the outer member has an infinite diameter, for example, the axial stress will vanish far away from the hole because of shear deformation. This effect is probably of little consequence since for increasingly large diameters, the forces and energies predicted in the analyses converge to specific values.

The two impact experiments showed a good correlation between the theory and data. Many more experiments must be done to determine how the weight of the impacting hammer affects the insertion produced. Experiments with pneumatic impact hammers should be done to see how accurate the analysis is for this situation, and whether the effect of preloads is similar to that derived by the quasi static analysis.

LIST OF REFERENCES

1. Nevins, J.L., et al., Exploratory Research in Industrial Modular Assembly, C.S. Draper Laboratory Report No. R-1111, August 1977.

2. Drake, S.H., Using Compliance in Lieu of Sensory Feedback for Automatic Assembly, Ph.D. Thesis, MIT Mechanical Engineering Department, September, 1977.

3. Shigley, J.E., Mechanical Engineering Design, McGraw-Hill, 1977, pg. 63.

4. Horger, O.J., "Press-and Shrink-fitted Assembly," Chapter 8, ASME Design Handbook, pp. 340-354.

5. Mechanical Design and Systems Handbook, McGraw-Hill, pp. 231 through 23-14.

6. Mark's Standard Handbook for Mechanical Engineers, McGraw-Hill, pp. 5-66,67; 8-62 to 8-64.

7. Jordan, R.L. Alan, "Designing Interference Fits," Machine Design, Vol. 46, No. 26, October 31, 1974, pp. 68-72.

8. Conway, H.D., and Farnham, K.A., "Contact Stresses Between Cylindrical Shafts and Sleeves," International Journal of Engineering Science, Vol. 5, 1967, pp. 541-554.

9. Steven, G.P., "The Shrink Fit Problem with Both Components Being Elastic," International Journal of Engineering Science, Vol. 13, No. 7-8, 1975, pp. 663-673.

10. Lindeman, Robert A., "Finite Element Computer Program for the Solution of Nonlinear Axisymmetric Contact Problems with Interference Fits," NWL Technical Report NWL-TR-3148, 1974.

11. Parsons, B., and Wilson, E.A., "A Method for Determining the Surface Contact Stresses Resulting from Interference Fits." Trans. ASME, Series B, Journal of Engineering for Industry, Vol. 90, pp. 208-218, February 1970.

12. Lamé and Clapeyron, "Memoire sur l'equilibre interieur des corps solides homogenes," Memoires presentes par divers savans, Vol. 4, 1833.

13. Rankin, A.W., "Shrink-Fit Stresses and Deformations," ASME Series E, Journal of Applied Mechanics, Vol. 11, No. 2, pp. A-77 through A-85, June, 1944.

14. Wilms, E.V., "Motion of an Elastic Rod with External Coulomb Friction," Trans. ASME Series B, Journal of Engineering for Industry, Vol. 90, p. 526, 1968.

15. Wilms, E.V., "Damping of a Rectangular Stress Pulse in a Thin Elastic Rod by External Coulomb Friction," Journal of the Acoustical Society of America, Vol. 45, pg. 1049, 1969.

16. Miller, R.K., "An Approximate Method of Analysis of the Transmission of Elastic Waves Through a Frictional Boundary," Trans. ASME, Series E, Journal of Applied Mechanics, Vol. 44, No. 4, December, 1977, pp. 652-656.